Smart Diaper With Printed Capacitive Sensors and Integrated Front-End to Monitor Voided Fluid Volume

Muhammad Tanweer, *Graduate Student Member, IEEE*, Dipesh C. Monga, *Graduate Student Member, IEEE*, Liam Gillan, Raimo Sepponen, I. Oguz Tanzer, *Member, IEEE*, and Kari A. I. Halonen, *Member, IEEE*

***Abstract*—As the demographic structure of the global population continues to shift toward an aging population, caregivers encounter formidable obstacles in detecting wetness events and assessing the quantity of voided volume within diapers. Nevertheless, the integration of electronics with diapers, frequent removal and reapplication, and battery management still pose practical challenges. In this study, a solution of carbon- and silver-printed flexible capacitive sensors interfaced with a custom-designed application-specific integrated circuit (ASIC) is proposed to detect urination events and estimate voided volumes in diapers. A power-optimized application-specific front-end interface circuit is developed to enhance power efficiency and reduce battery maintenance. The circuit is designed to support power-harvesting-based operations and to reduce reliance on external sources, consuming a maximum power of 3.05 μW. In vitro measurements validate on-chip electronics functionality and sensor performance to detect and quantify voided fluid volume as low as 50 mL. The promising results pave the way for cost-effective, disposable solutions in smart diapers. The proposed solution improves efficiency and comfort for both caregivers and elderly individuals.**

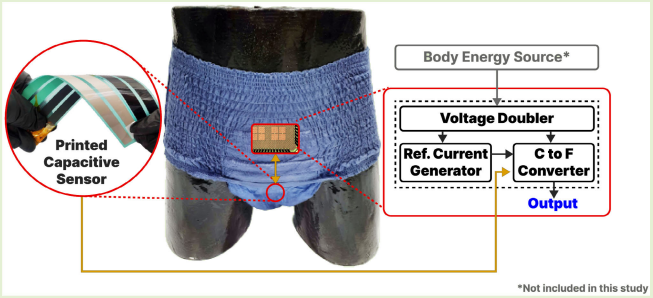

***Index Terms*—Coplanar capacitive sensors, disposable electronics, energy harvesting, printed electronics, smart diapers, voided volume of urine.**

I. Introduction

EUROPE is one of the most rapidly aging regions because of enhanced life expectancy and declined fertility rates. It is estimated by the United Nations (UNs) that by mid 21st century, 30% of the European Union (EU) population will be 60 years and above. The share of the EU in the global population has declined to 50% in the last half-century and is expected to decline further at the same rate [1]. The aging population has caused a hype in demand for healthcare services and systems. Urinary incontinence, also defined as involuntary urination, is one of the most common problems associated with the elderly population because of an overactive bladder, stress, and diseases such as dementia and diabetes [2].

The development of disposable hygiene products has improved the quality of care provided to elderly population. Nonwoven pad-type adult diapers are vastly used by care providers to address urinary incontinence-related challenges among the geriatric population to maintain better hygiene [3]. Elderly people receiving care feel embarrassed to discuss incontinence issues and ask for help because of social and psychological pressure [4], [5].

Urinary parameters are vital to monitor as they offer valuable and sensitive information about health status and conditions, including kidney function, hydration levels, dietary habits, and the possible presence of certain health issues [6]. In current practice, the care providers have to check diapers hourly for wetness and weigh them on the conventional scales to evaluate the voided volumes. Furthermore, paper charts and bladder diaries of voided volumes are maintained conventionally [7], hence overburdening the jobs of care

Manuscript received 15 February 2024; accepted 20 March 2024. Date of publication 28 March 2024; date of current version 1 May 2024. This work was supported by the Urisens Project through Business Finland under Grant 1696/31/2022 and in part by the EHIR Project through Academy of Finland under Grant 13334487. The associate editor coordinating the review of this article and approving it for publication was Dr. Hui Jiang. *(Muhammad Tanweer and Dipesh C. Monga contributed equally to this work.) (Corresponding author: Muhammad Tanweer.)*

Muhammad Tanweer, Dipesh C. Monga, Raimo Sepponen, I. Oguz Tanzer, and Kari A. I. Halonen are with the Department of Electronics and Nanoengineering, Aalto University, 02150 Espoo, Finland (e-mail: muhammad.tanweer@aalto.fi).

Liam Gillan is with the VTT Technical Research Centre of Finland Ltd., 02150 Espoo, Finland (e-mail: liam.gillan@vtt.fi).

Digital Object Identifier 10.1109/JSEN.2024.3380890

providers. Delays in a diaper change and prolonged exposure to diaper liquids cause overhydration of the skin resulting in diseases such as incontinence-associated dermatitis leading to more serious genital bacterial infections and urinary tract infections (UTIs) in geriatric people [8], [9], [10], [11], [12].

Advancements in wearable biomedical devices have enabled long-term monitoring of physiological parameters and seamless transmission of data to the cloud using the Internet of Things (IoT) [13], [14]. A Bluetooth-based in-diaper UTI detection system is developed by [15], which deploys the colorimetric nitrite sensor with urine-based batteries. A neonatal jaundice sensor is developed by [16] using zinc oxide nanoarray to create hydrovoltages in diapers. Similarly, to address the incontinence issues, various urination detection systems are developed for diapers using off-the-shelf wireless communication modules such as GSM [17], Bluetooth [18], [19], and RFID [20], [21], [22].

Various types of wetness sensor developments are presented in the literature to detect urination events in diapers. Resistive sensors are used to detect wetness in diapers in [17], [18], and [23]. A hydrogel-based RFID tag is introduced in [21] to detect the wet and dry diapers by placing the reader at 30 cm. In another technique, voltage sensors are used to detect urination events in diapers using off-the-shelf components [20]. However, quantification of urination and detection of multiple urination events is challenging with resistive sensors, and the readings from hydrogel antennas are affected by the change in reader orientation and distance from the sensor hence making it challenging for practical applications that require quantification of voided volume.

The capacitive sensors in coplanar orientation are widely used in literature for the measurement of relative permittivity to characterize various materials. It is used by [24], [25], [26], and [27] to detect moisture levels in the soil, by [28] to characterize ethyl-acetate, butyraldehyde, isopropanol, and ethanol. These coplanar capacitive sensor structures are also commonly used for urination detection in diapers [16], [22], [29], [30], [31]. In a study, a capacitive sensor made of conductive blades is used to quantify the urine volume in a voiding container [32]. The capacitive sensing technique provides better urination detection and quantification of voided volume when compared with other sensing techniques. The advancements in printed electronics technology have made it possible to develop sensors and circuits on flexible and foldable substrates using sustainable and biodegradable materials [33], [34].

Compared with smart diapers developed using off-the-shelf components [17], [18], [19], [29], to the best of our knowledge, this study is the first report involving a printed sensor integrated inside a diaper and interfaced with a dedicated ultralow-power application-specific integrated circuit (ASIC) front-end to run on an energy harvesting source by eliminating the need of batteries. The capacitive sensors are printed using silver and carbon inks on flexible substrates in coplanar orientation based on the recommendations of [30], [31], and [32]. The capacitive sensors enhance the quantification of voided fluid volume and introduce the capability to detect multiple urination events in the same diaper when compared with resistive sensing technique [17], [18], [23]. The capacitive sensors are integrated inside the diaper to reduce the impact of the external materials in close proximity on capacitive sensors which is experienced when positioned outside of the diaper [22].

An analog front-end is developed by incorporating a capacitance-to-frequency converter using the state-of-the-art complementary metal oxide semiconductor (CMOS) technology to interface with printed capacitive sensors on flexible substrates. The analog front-end is featured with a power-optimized circuit design, making it suitable for energy-harvesting-based battery-less operations. The elimination of bulky off-the-shelf components leads to an improved form factor and lower power consumption. There is no need to provide training to care providers for device replacement and battery management, hence improving operation efficiency, reducing the work, and improving comfort by adding convenience use which is faced by 41% of respondents in [18]. A current-controlled capacitance-to-frequency converter is used to detect changes in the sensor capacitance. The integrated front-end can be powered by an energy harvester obtaining its energy from active and passive human body energy sources such as heat-driven thermoelectric generators [35], [36], urine [37], and other various energy sources. The interface circuitry is designed in a 65-nm bulk CMOS technology and a set of comprehensive measurements have been conducted to characterize the circuit's performance.

This study uses sustainable and economical printable carbon ink for the development of carbon sensors when compared with [22], [29], [31], and [32]. Capacitance-to-frequency conversion technique is adopted in ASIC design instead of capacitance-to-voltage conversion [31], [32] to create the possibility for more robust digital designs of cascaded integrator comb filter to perform the frequency-to-digital conversion as proposed by [38] instead of using power-hungry and complex circuits as analog-to-digital converters.

The development of printed capacitive sensors on flexible substrates, the design details of the analog front-end with power management, and the experimental setup are discussed in Section II of this article. Section III discusses the measurement results by showcasing graphs, charts, and tables. Finally, Section IV summarizes the study by discussing the findings, implications, limitations, and potential future research.

II. System Architecture

A. Coplanar Capacitive Sensor

In this study, capacitive sensors with electrodes in coplanar orientation are used. The design of coplanar capacitive sensors is presented in Fig. 1(a) where two electrodes of width (W) and length (L) are printed using conductive ink on a substrate having thickness (h) at a given interelectrode distance (D). The relative permittivity of the substrate is ε_r. The thickness of printed electrodes (t) is less than 10 μm and the thickness of printed insulator (m) is tens of micrometers. The capacitance of the printed sensor can be defined with (1) by assuming the thickness of electrodes and insulator is zero and by considering the fact that the value of constant K is between 0 and $(1/\sqrt{2})$ [39]. Equation (1) shows that sensor capacitance

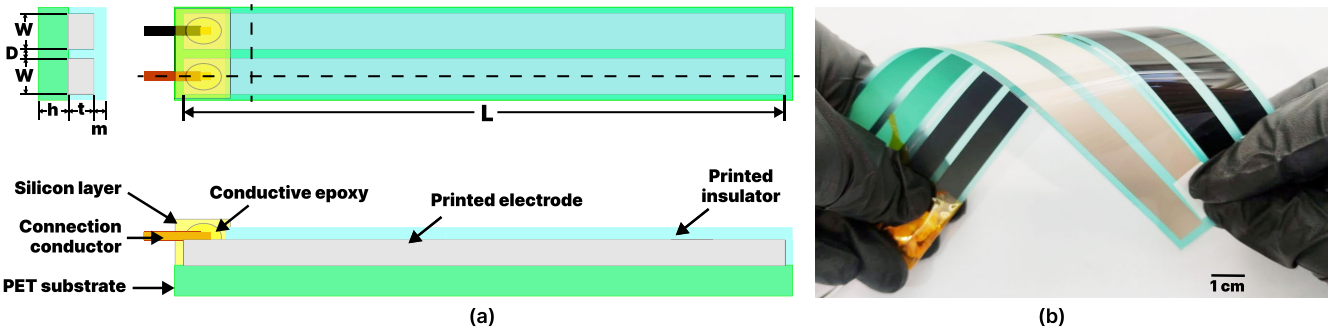

(a) (b)

Fig. 1. (a) Coplanar capacitive sensor design using printed technology. (b) Sensors fabricated with screen-printing technology using silver and carbon inks.

C_{sensor} is directly proportional to the effective permittivity ε_r' of the medium, hence making the coplanar configuration of electrodes suitable to detect the significant variations in relative permittivity of the medium as is the case of urination event in adult diaper

$$C_{\text{sensor}} = \frac{\varepsilon_r' \ln\left(2 \times \frac{1+\sqrt{K}}{1-\sqrt{K}}\right) \times L}{377\pi\, v_0} \tag{1}$$

where

$$K = \sqrt{1 - \left(\frac{D}{D+2W}\right)^2} \tag{2}$$

$$\varepsilon_r' = \frac{\varepsilon_r + 1}{2}\left\{\tanh\left[0.775 \times \ln\left(\frac{h}{W}\right) + 1.75\right] + \frac{KW}{h} \times [0.04 - 0.7K + 0.01(1 - 0.1\varepsilon_r)(0.25 + K)]\right\} \tag{3}$$

and

$$v_0 = \frac{1}{\sqrt{\mu_0 \varepsilon_0}}. \tag{4}$$

The ε_r' of the medium is calculated using (3) when the sensor is placed in the medium having a homogeneous distribution of the electric field. The h in (3) represents the thickness of super absorbent polymer (SAP) having ε_r of 9 [40] in dry conditions and thickness of liquids having ε_r of 80.1 in wet conditions. The capacitance of the printed sensor with W of 10 mm, L of 200 mm, and D of 3 mm placed on SAP material having h of 4 mm is calculated as 14.7 pF. This represents the capacitance of the sensor when it is placed in a diaper in a dry condition.

1) COMSOL Model of Sensor: The model of the coplanar capacitive sensor is developed using the COMSOL Multiphysics simulation tool to analyze the behavior of the sensor in various media. Computational algorithms of the COMSOL tool are used to evaluate the capacitance of the sensor. In the COMSOL model, two electrodes with W of 10 mm and L of 200 mm are placed in coplanar orientation with D of 3 mm. The bottom side of coplanar electrodes is encapsulated with 39-μm insulators having ε_r of 3.99 [41]. A substrate of polyethylene terephthalate (PET) material having h of 125 μm with ε_r of 4.0 is used above the electrodes [42]. A block of 30-cm length, 10-cm width, and 4-mm thickness having ε_r between 3 and 9 [40] is used above the sensor to mimic the SAP material of the diaper pad. The sensor model is placed in a spherical medium of radius 30 cm to study the electrical potential distribution in various materials. Fig. 2(a) shows the cross section of zoomed capacitive sensor model. Fig. 2(b) shows the 3-D model of the sensor placed in a spherical medium.

The electrodes of the sensor are set to an electric potential difference of 1 V. Fig. 2(c) depicts the electrical potential distribution in the air medium with ε_r of 1 when electrodes on PET substrate are encapsulated with a printed insulator and the calculated capacitance is 4.6 pF. Fig. 2(d) represents the electric potential distributions when the sensor is placed under the SAP block having a ε_r of 9 and the calculated capacitance is 15.5 pF. The calculated capacitance is 105.1 pF when the SAP block is replaced with a water block of the same dimensions having a higher ε_r of 80.1. The distribution of the electric potential is shown in Fig. 2(e). The capacitance increased to 170.3 pF when the fluid block thickness is increased from 4 mm to 4 cm and increased further to 274.6 pF when the spherical air medium of 30 cm is replaced with water.

In the simulation results, it is observed that sensor capacitance measures less than 20 pF in a dry diaper environment. There is a significant increase in sensor capacitance when the SAP block of the dry diaper is replaced with a fluid having high relative permittivity. The distribution of the electric potential is denser in the media with higher relative permittivity.

2) Fabrication of Sensors: Coplanar capacitive sensors with the same geometry as described in Section II-A are produced by sequential deposition and curing of electrically conductive silver (Asahi LS-411AW, oven-dried at 120 °C for 20 min) or carbon (Sun C2171023D1, oven-dried at 130 °C for 30 min), followed by encapsulation with insulator (Loctite EDAG PF 455B E&C, two layers sequentially printed and ultraviolet (UV) light-cured with a fusion UV light systems D-bulb for 2 min per layer). All the ink layers are printed onto sheets of PET substrate (Dupont Teijin Films, Melinex ST506, 125 μm thick) using a flat bed screen printer (EKRA, E2) and stainless-steel screens (Finnseri OY) with a wire diameter of 28 μm and a mesh count of 328 lines per square inch. Printed layers are manually registered using a camera module. The thickness of the printed films (silver ~9 μm, carbon ~5 μm, insulator ~39 μm) is determined using a confocal microscope (SensoFar, S Neox 3-D optical profiler). The

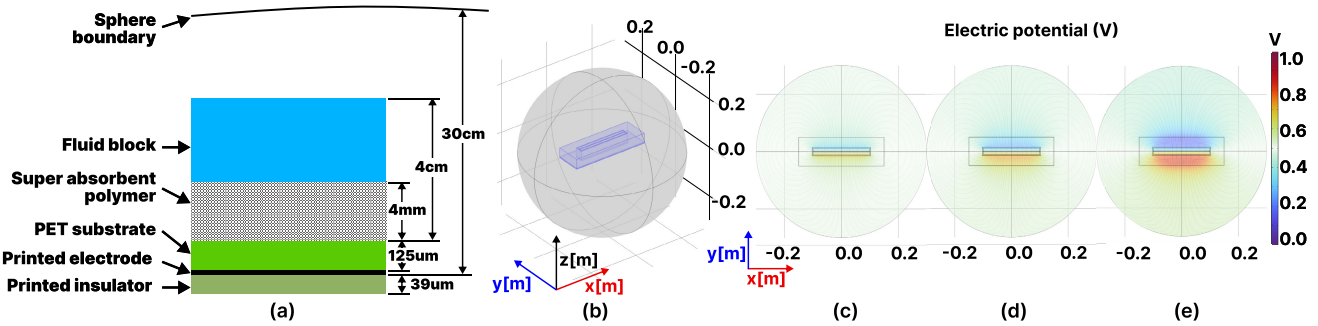

Fig. 2. (a) Cross section of zoomed capacitive sensor model in COMSOL. (b) Model of capacitive sensor deployment into medium. (c) Electric potential simulations of the sensor on a substrate with the printed insulator. (d) Electric potential simulations sensor in SAP material of 4 mm. (e) Electric potential simulations sensor in water 4 mm.

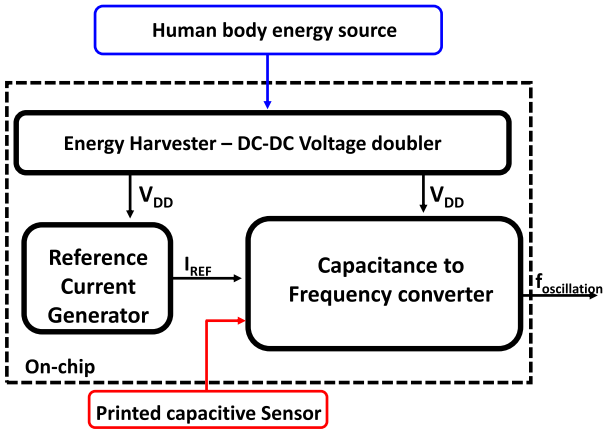

Fig. 3. Analog front-end description of the proposed circuit.

sheet resistance of the printed conductive features is measured using a four-point probe (A&M Fell, Model B) connected to a multimeter (Keithley 2001) to obtain ∼2 mΩ/□ and ∼18 Ω/□ for printed silver and carbon films, respectively. The connection conductors are attached to the printed electrodes with two-part conductive epoxy (Chemtronics CW2400, oven-dried at 90 °C for 5 min). The electrical connections are secured with silicone paste (Bison 6305449, cured at room temperature for 24 h) to achieve waterproofing and mechanical strength. The finished version of silver- and carbon-printed capacitive sensors is presented in Fig. 1(b).

B. Design and Implementation of Analog Front-End

The overview of the analog front-end for detection of voided volume is shown in Fig. 3. The circuit sensing the capacitance consists of a constant reference current generator that provides a temperature-invariant current, and a current-controlled ring oscillator (RO) is implemented for capacitance-to-frequency conversion. The capacitance-to-frequency converter generates a frequency dependent on the capacitance of the off-chip capacitive sensor. These analog blocks are powered by a switched-capacitor-based cross-coupled voltage converter doubling the voltage from a stable external source.

1) Capacitance-to-Frequency Converter: A five-stage current-starved, current-controlled RO consisting of inverters INV_1–INV_5 is used to sense the changes in the off-chip capacitive sensor as shown in Fig. 4(d). This circuit is used due to its simplicity, linearity, and frequency-based output. The reference current, I_{REF} for the oscillator, can be obtained from an on-chip or off-chip current reference. The reference current is mirrored from metal oxide field-effect transistor (MOSFET) M_{N2} to same-sized transistors M_{N3}–M_{N6} (I_N). For the PMOS transistor, the current I_P is mirrored from M_{P1} to identical transistors M_{P2}–M_{P6}. The mirroring transistors are sized to have both I_P and I_N equal to an average of the input reference current I_{IREF} i.e.,

$$I_P = I_N = I_{REF}/2. \tag{5}$$

The relationship between I_P, I_N, and I_{ref} can be controlled by the mirroring ratio of M_{N1} to $M_{N2} - M_{N7}$ and similarly it can be done for PMOS. An I/O pad for the off-chip capacitive sensor is connected at the output of the first stage of the inverter INV_1 (C_{INV1}) (discussed in Section II-B2). The propagation delay of this inverter is defined by the capacitance of the inverter in parallel with the off-chip capacitive sensor and the interconnect parasitic capacitance C_{para}. In the subsequent stages, C_{INV} is the output capacitance of the inverter of each stage of INV_2–INV_5. A buffer inverter INV_6 of minimum aspect ratio is used in the last stage to improve the stability of the output waveform. The time period of oscillation (T) is given as

$$T_{oscillation} = 2(t_{delay1} + t_{delay2} + t_{delay3} + t_{delay4} + t_{delay5}) \tag{6}$$

where N is the total number of stages (i.e., 5), and t_{delay} is the propagation delay of each inverter stage denoted by their subscript and is given by the sum of the stage delay and the charging time of the capacitor and the factor 2 results since a complete cycle requires a low-to-high and high-to-low transition of the signal. Note that each inverter stage's capacitance (C_{INV}) is the same as equal-sized inverters are used.

The output frequency of capacitance-to-frequency converter $f_{oscillation}$ is given by

$$f_{oscillation} = \frac{I_{REF}}{2(5C_{INV} + C_{para} + C_{sensor})V_{DD}} \tag{7}$$

where C_{sensor} is the capacitance of the off-chip sensor, and V_{DD} is the supply voltage from the voltage doubler output. The supply voltage for this application, obtained from the human body energy sources discussed, remains constant during the

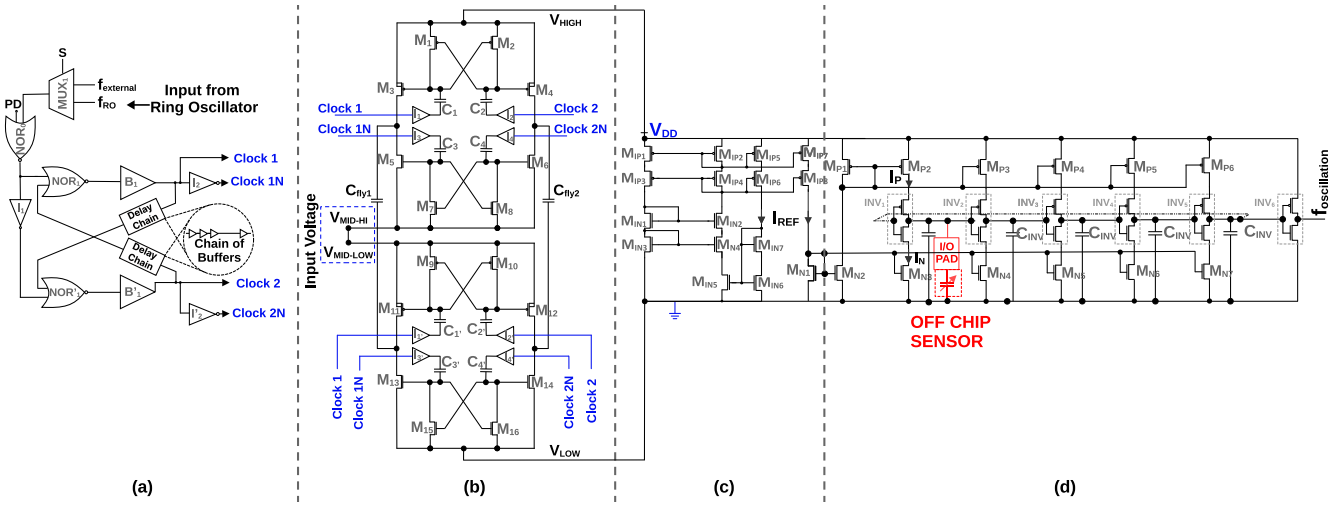

Fig. 4. Circuit diagram of the analog front-end depicting the circuit of (a) NOL generator, (b) voltage doubler, (c) reference current generator, and (d) capacitance-to-frequency converter.

operation time. Hence, this circuit does not require the need for a regulator; if the supply is not stable, then voltage regulators can be used. The frequency in (7) is calculated by the total time taken to charge the inverter load capacitors from zero to V_{DD}. Therefore, the output frequency changes inversely with the change in C_{SENSE}. The circuit consumes power of 0.8–2.5 μW with C_{SENSE} ranging from 5 to 200 pF. The circuit has an operating voltage range of 0.8–1.3 V, and a nominal operation voltage of 1.2 V, at a reference current I_{ref} of 100 nA.

2) Current Reference Generator: A key factor for a clock generator's performance and reliability is its current reference's stability. To obtain a stable frequency for capacitance-to-digital conversion, a beta-multiplier-based current reference is used in this system. This circuit has good thermal stability with a low process variation and is less sensitive to variations in the supply voltage. The current reference enhances phase noise performance, frequency accuracy, and frequency robustness in the capacitance-to-frequency converter.

A resistorless beta-multiplier adapted from [43] has been used in this circuit to generate a thermally invariant current as shown in Fig. 4(c). In this circuit, the resistors are replaced by MOS cascode transistors M_{NI5} and M_{NI6}. The bias voltage required for the MOSFETs to operate in the linear region is generated from NMOS M_{NI7}. I_{REF} is the bias current generated by the circuit. To improve the line sensitivity, each branch of the circuit has cascode current sources consisting of M_{PI1} and M_{PI3}, M_{PI2} and M_{PI4}, M_{NI1} and M_{NI3}, and M_{NI2} and M_{NI4}. The thermal stability of the circuit is achieved by careful sizing of transistors M_{NI5}–M_{NI7}. The temperature dependence of the current is influenced by several factors, including the threshold voltages of M_{NI5}–M_{NI7}, as well as the carrier mobility and thermal voltage. These parameters collectively contribute to the temperature sensitivity of the circuit.

The relationship between threshold voltage and temperature is complementary to absolute temperature (CTAT). This means that adjusting the aspect ratios of a circuit can alter its CTAT behavior. On the other hand, carrier mobility and thermal voltage contribute to the proportional to absolute temperature (PTAT) dependence. A thermally compensated output current is obtained by selecting aspect ratios that counterbalance the temperature dependence of mobility with the temperature dependence of threshold voltage.

The designed current reference circuit generates a current of approximately 100 nA and has a temperature coefficient of 48 ppm/°C for a temperature range of −40 °C to 85 °C at an operating voltage of 1.2 V with a power consumption of 0.55 μW at room temperature. The line sensitivity (%/V) of this circuit is 1.9 %/V with a process variation ($3\sigma/\mu$) of 4%.

3) Voltage Doubler: Due to its inherent advantages such as reduced component count, simplicity of design, and improved efficiency at lower output currents, a cross-coupled voltage doubler is used to harvest and regulate the output voltage to the capacitance-to-frequency converter and the current reference. The circuit is a reconfigurable cross-coupled switched capacitor two-phase interleaved dc–dc converter based on [44], [45]. The cross-coupled scheme is used to double the input voltage from an energy source, and the two phase scheme reduces the output ripple due to the interleaving of the cross-coupled stages, thus regulating the output. This circuit can provide voltage conversion ratios of 1:2 or 2:1, depending on the input and output connection to its terminal.

Furthermore, the two-phase interleaved clocks are implemented by an on-chip RO that generates a system clock to generate two-phase nonoverlapping (NOL) clocks, Clock 1 and Clock 2, with their inverted output Clock 1 N and Clock 2 N, respectively. Fig. 4(a) shows the NOL clock generator circuit. The circuit is realized by a combination of NOR gates, delay buffers, and inverters. The input clock signal to the circuit is provided either from an on-chip RO or from an off-chip clock generator; this selection can be done by MUX_1. Furthermore, a power-down (PD) signal can be used to turn ON/OFF this NOL clock generator. The input clock signal from the RO and its inverted form is fed to the two-input NOR gates NOR_1 and NOR'_1, and the second input for the NOR gates is fed with delay chains blocks comprising a chain

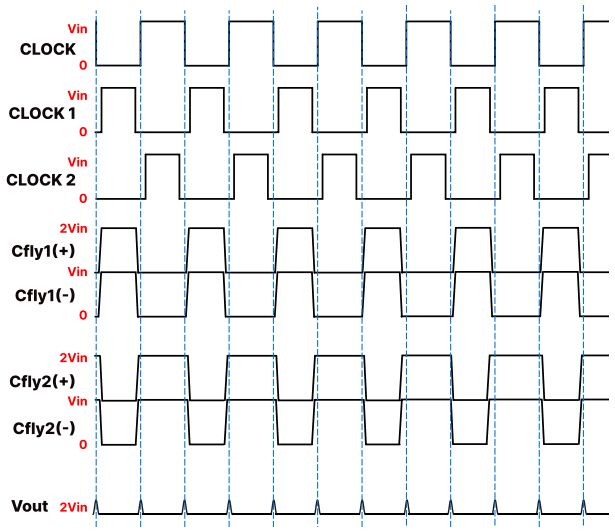

Fig. 5. Timing diagram depicting the clock phases generated by the NOL clocks, voltages at the terminals of flying capacitors, and the output voltage (Vout).

of buffers. This delay chain in the circuit provides a delay for the output to realize the NOL time, which can be controlled by the number of buffers.

The dc–dc converter has four terminals for input and output connections, namely, V_{HIGH}, $V_{\text{MID-HIGH}}$, $V_{\text{MID-LOW}}$, and V_{LOW} as shown in Fig. 4(b). For this application, the input voltage is obtained from an active or passive human body energy source providing a dc voltage of 0.6 V [35]. The circuit is used as a voltage doubler (1:2). In this case, the input voltage Vin is connected to $V_{\text{MID-HIGH}}$ and $V_{\text{MID-LOW}}$ terminals. The V_{HIGH} terminal is connected to the output loads, i.e., reference current generator and capacitance-to-frequency converter, providing them with a constant supply of 1.2 V.

In the circuit, the body of PMOS M_3, M_4, M_{11}, and M_{12} is connected to their source, which reduces the channel leakage. The transistor's threshold voltage can be effectively controlled by adjusting the bulk bias voltage to reduce conduction and leakage losses as presented in [46]. This allows the converter to operate in its most efficient region for different load conditions, hence improving overall energy efficiency.

Capacitors C_1 to C_4 and $C_{1'}$ to $C_{4'}$ are bootstrap capacitors to boost the gate voltages of the switches M_1 to M_8. The flying capacitors Cfly1 and Cfly2 drive the output loads and are much larger than the bootstrap capacitors. Fig. 5 shows the in-detail timing diagram of the NOL clocks and the output voltage at the positive and negative terminals of the capacitors and the overall output voltage Vout with the ripples. The bootstrap capacitors are 0.5 pF each, and the flying capacitors are 200 pF each. The buffers $I1$-$I4$ and $I1'$-$I4'$ are powered by the output voltage of the voltage doubler V_{HIGH} to ensure rail-to-rail switching of the MOS transistors.

The interleaving of two converter phases allows the flying capacitor to overlap their charge and discharge cycles, ensuring a more continuous flow of charge between capacitors. When one stage charges a flying capacitor, another can simultaneously discharge the other flying capacitor. This overlapping of cycles significantly reduces the idle time and energy loss associated with traditional noninterleaved converters. In addition, the output ripple voltage is reduced as the two phases cancel out the ripples because of overlap. Moreover, this circuit reduces the need for a larger output capacitor as a smaller output capacitor, or even no capacitor at all, can be used due to the significantly reduced ripple. Therefore, in this work, no output capacitor has been connected to the load.

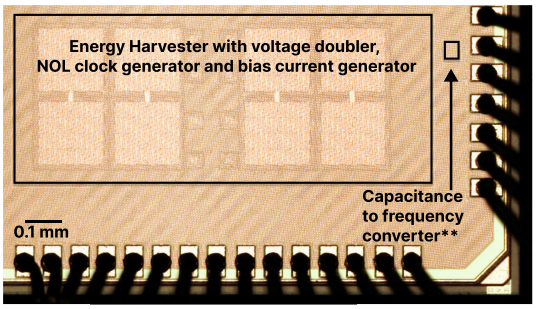

Fig. 6. Die micro-photograph of the implemented analog front-end containing the current reference generator, NOL clock generator, and capacitance-to-frequency converter circuit. **Approximate location due to the presence of layer masks.

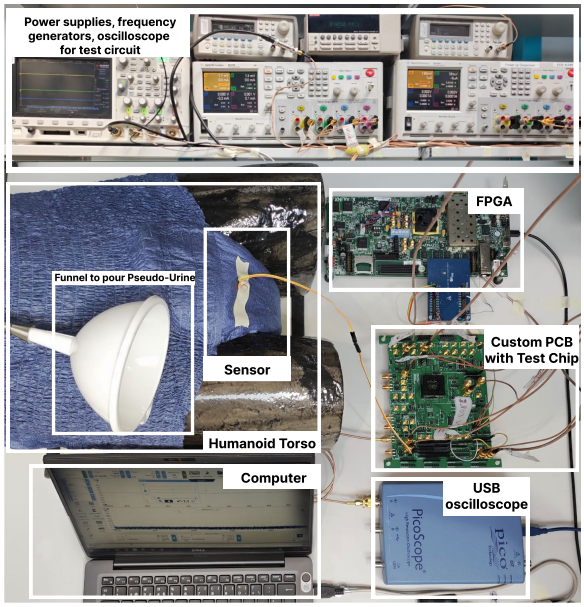

Fig. 7. Experimental setup showcasing in-diaper capacitive sensors deployed on a horizontally positioned human torso, emulating a lying position.

C. Experimental Setup

1) Analog Front-End Validation Measurements: The analog front-end is implemented in a 65-nm bulk CMOS process. A micro-photograph of the designed chip and the layout of the implemented circuit is shown in Fig. 6. The overall system, along with the energy harvester, occupies an area of 0.8 mm^2, including the I/O pads (0.375 mm^2, without I/O pads).

The measurement setup used to characterize the test chip with the analog front-end is shown in Fig. 7. The setup consists of a frequency generator (Agilent-33220A) to generate a clock for the SC dc–dc converter, a dc power analyzer (Agilent-N6705B) to provide input voltage (emulating a body energy source) and I/O pad supplies, a Xilinx FPGA (XC7Z045 of ZYnQ-7000 series) to communicate with the serial peripheral interface of the test chip, and an oscilloscope (PicoScope-4262, Pico Technology) to measure the output

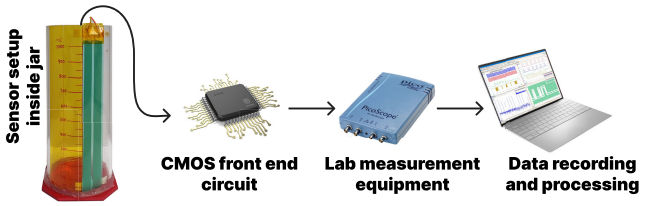

Fig. 8. Integration of printed capacitive sensors with analog front-end measurement setup for in-jar measurements.

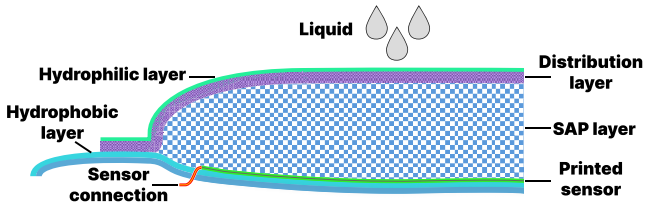

Fig. 9. Cross section illustration of an adult diaper with an integrated flexible capacitive sensor.

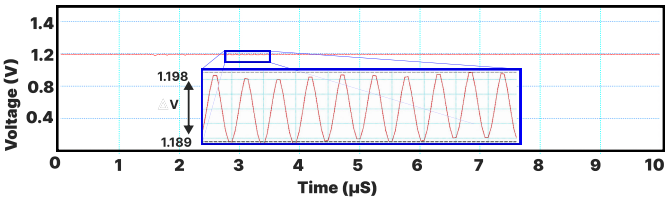

Fig. 10. Measured output of the voltage doubler circuit along with the output ripples providing insight into the small variations observed around the stable output voltage.

frequency of the on-chip RO and to measure the ripples of the voltage doubler. The power supply devices and the measurement instruments are connected to a custom printed circuit board (PCB) designed to characterize the test chip.

An input voltage source to emulate the energy source is used to characterize the voltage doubler. The output of the voltage doubler is then connected to V_{DD} pad of the capacitance-to-frequency converter, powering the circuit. The operation of the on-chip capacitance-to-frequency converter is validated with the measurement setup established in Fig. 7. A wide-range programmable digital capacitor (NCD2400M) by IXYS Integrated Circuits Division is deployed on an Arduino platform to substantiate the functionality of the capacitance-to-frequency converter. With an on-chip input current I/O pad to the capacitance-to-frequency converter, the input current can be provided externally to characterize the output frequency dependence on the input current. Alternatively, the on-chip current reference can be used to provide a temperature, voltage, and process-invariant current. After establishing the connection, the initial measurements are initiated by adjusting the input capacitor while recording the resulting frequency. Subsequently, the digital capacitor is substituted with the capacitive printed sensors for fluid detection and quantification.

2) Sensor Integration and Measurements: In this study, measurement scenarios are planned for the in-jar and the in-diaper deployment of printed capacitive sensors integrated with the analog front-end. Silver- and carbon-printed capacitive sensors are used in both the measurement scenarios. For the in-jar measurement scenario, the silver- and carbon-printed capacitive sensors are one by one deployed in a vertical jar with a capacity to hold 1 L of fluid. The integration layout of printed capacitive sensors for in-jar measurement setup with analog front-end is depicted in Fig. 8. The change in the relative permittivity of the sensor medium causes a change in the capacitance, hence resulting in a change in the output frequency of the analog front-end.

For the in-diaper measurement scenario, the silver- and carbon-printed capacitive sensors are one by one deployed inside the adult diapers. The cross-section illustration of an adult diaper and the sensor placement under the SAP layer of the diaper is shown in Fig. 9. The hydrophilic layer provides easy absorption capability and the distribution layer spreads the fluid uniformly over the SAP layer. The hydrophobic layer is responsible for keeping all the fluid inside the diaper and prohibits leakages. The flexible capacitive sensor is deployed directly above the hydrophobic layer and right below the SAP layer to achieve effective sensing and quantification capability.

In the first in-diaper measurement scenario, the wet diaper detection and in-diaper fluid quantification measurements are performed for silver and carbon capacitive sensors in a controlled laboratory table environment. An adult diaper pad is used with a capacity to hold a voided volume of 300 mL. A second in-diaper measurement scenario is devised in a controlled laboratory environment where silver and carbon sensors are deployed one by one into adult diapers on a humanoid torso emulating lying position. The wetness event detection, intermittent urination event detection, and over time wet diaper effects on printed sensors are analyzed.

III. Results and Discussion

The validation measurements are performed using the experimental setup as shown in Fig. 7. First, the voltage doubler is measured by emulating an input voltage from energy harvester of 0.6 V and using a dedicated on-chip RO at an operating frequency of 1 MHz, with 1.2-V peak-to-peak amplitude to power the capacitance-to-frequency converter. As depicted in Fig. 10, the output voltage exhibits a ripple of 9 mV when supplied with an input voltage of 0.6 V and generates an output voltage of 1.2 V. Moreover, the voltage doubler demonstrates its capability to handle a load up to 26 μW and achieves a peak efficiency of up to 91.4%. The measurement results of the voltage doubler signify its compatibility and performance to ensure reliable power delivery to the capacitance-to-frequency converter.

The capacitance-to-frequency converter is characterized by the programmable digital capacitor from 10 to 210 pF to emulate the capacitive sensor in the dry and wet states. The input current is set at 50, 100, and 150 nA progressively to analyze the frequency response of the capacitance-to-frequency converter. The measurement results are presented as capacitance versus frequency curve in Fig. 11. It is observed that the higher input current results in better frequency response at high capacitance values of the sensor. The on-chip current reference of 100 nA is used for the capacitance-to-frequency converter for this study to achieve power-optimized operation and still have enhanced frequency response.

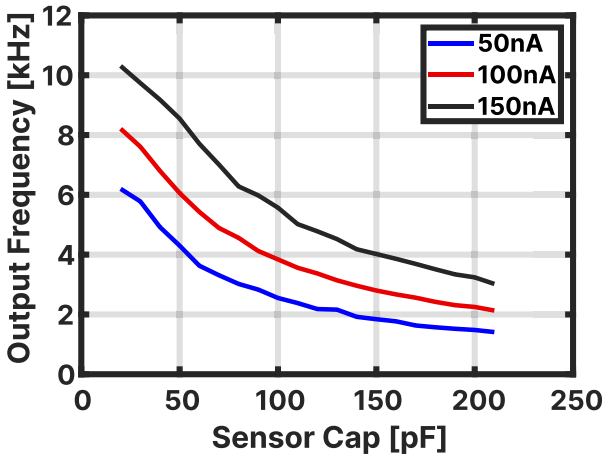

Fig. 11. Validation of capacitance-to-frequency converter with programmable input sensor capacitance on various input reference currents.

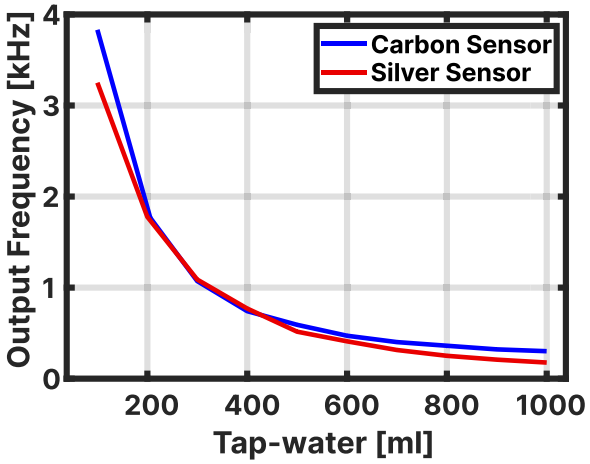

Fig. 12. In-jar tap water quantification measurements with 100-mL increment using capacitive sensors printed with carbon and silver ink.

For the in-jar measurement scenario, the jar is filled with tap water up to 1 L into the jar with an increment of 100 mL for each measurement of silver and carbon sensors. The output frequency of the analog front-end is recorded as 8.15 kHz for the silver sensor and 8.68 kHz for the carbon sensor inside the jar during dry conditions. The frequency change response to the change in water level inside the jar during wet conditions for silver and carbon sensor is presented in Fig. 12. It is observed that the frequency curve follows the $1/C$ dependence as described in (7). The carbon sensor has recorded lower capacitance when compared with the silver sensor because of more sheet resistance thus producing higher output frequencies for the same level of fluid. However, both the sensors have yielded similar behavior toward the changes in fluid quantity. An increase in the fluid level in the jar has an inverse relationship with the output frequency of the analog front-end.

In the first in-diaper measurement scenario, the dry and wet diaper detections are performed before and after the introduction of 300 mL water into the diaper. The detection results for both silver and carbon sensors are tabulated in Table I. The output frequency of the analog front-end is observed to be above 8 kHz for both silver and carbon

TABLE I
CAP SENSORS DEPLOYED INSIDE DIAPERS FOR DRY AND WET ANALYSES

Cap-sensors	Dry	Wet
Silver Sensor	8.13 kHz	0.59 kHz
Carbon Sensor	8.16 kHz	0.39 kHz

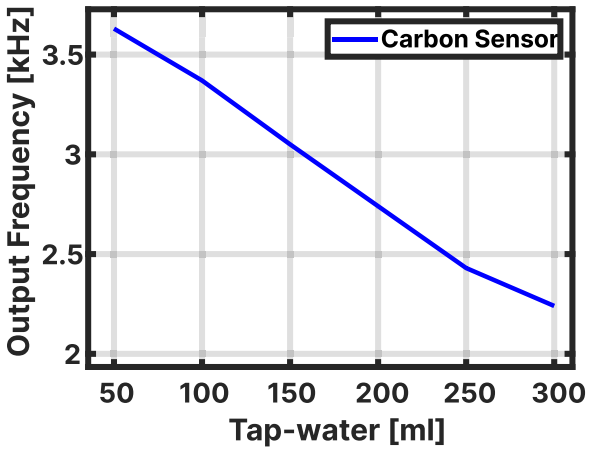

Fig. 13. In-diaper tap water quantification measurements with 50-mL increment using carbon-printed capacitive sensor.

sensors in dry diaper conditions. The frequency is dropped significantly from 8 kHz to lower than 1 kHz in wet diaper conditions for both silver and carbon sensors when 300 mL fluid is introduced to the diaper. The same measurement setup is used for the quantification of voided volumes inside sensor-integrated adult diapers. The 300 mL of tap water is introduced to the diaper pad with an increment of 50 mL and the measurement is performed after 30 s settling time of each increment. Based on the in-jar quantification measurement results, only the printed carbon sensor is used for tap water quantification measurement as both the sensors show similar behavior toward the changes in fluid volumes. The quantification results of voided volume by carbon sensor are plotted in Fig. 13. A linear drop of about 1.5 kHz in the output frequency is observed when tap water volume increased from 50 to 300 mL.

In another set of quantification measurements, the tap water is replaced with the synthetic urine (60 mmol/L solution of table salt, NaCl), and the poured volume is changed with a 50-mL incremental step up to 300 mL. The results from both the carbon sensor and silver sensor are presented in Fig. 14. The silver sensor results in a frequency change of about 3 kHz, and the carbon sensor results in a frequency change of about 5 kHz because of the variation in the sheet resistance of both inks. It is also observed that the printed carbon capacitive sensor reads higher frequency values in synthetic urine when compared with water. The variable concentration of electrolytes in voided same voided volume yields different results for capacitive sensors, and the gravitational pull on the wet diaper and body weight also causes variation in the capacitance readings. The parameters from additional sensors such as electrolyte concentration sensors, pressure sensors, and torso orientation sensors might be considered to compensate for the variations to enhance the precise quantification of the voided volume in adult diapers as discussed by [47].

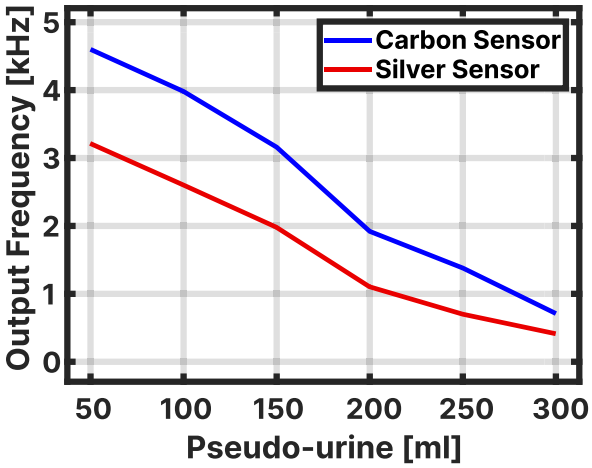

Fig. 14. In-diaper synthetic urine quantification measurements with 50-mL increment using silver- and carbon-printed capacitive sensor.

TABLE II
TIME EFFECT ON A WET DIAPER ON THE HUMANOID TORSO EMULATING LYING POSITION

Cap-sensors	1 min	5 min	10 min
Silver Sensor	5.19 kHz	5.46 kHz	5.80 kHz
Carbon Sensor	7.01 kHz	7.06 kHz	6.97 kHz

TABLE III
DETECTION OF INTERMITTENT FLUID IN THE DIAPER ON THE TORSO EMULATING LYING POSITION

Cap-sensors	1st Pour	2nd Pour
Silver sensor	4.97 kHz	1.89 kHz
Carbon sensor	7.01 kHz	4.52 kHz

In the second in-diaper measurement scenario, both silver and carbon sensors are integrated into adult diapers on a humanoid torso in a controlled environment. The time effect on quantification is measured for a wet diaper on a humanoid torso emulating lying position. Fig. 7 shows the measurement setup with the humanoid torso. The water quantity of 100 mL is poured into the diaper and measurements of analog front-end output frequency are recorded at 1-, 5-, and 10-min time-lapse. The results are tabulated in Table II. A slight increase in the output frequency of the analog front-end is observed over time. The liquids are also soaked by SAP material in diaper areas away from the sensor over time to distribute the voided volume uniformly, hence causing a decay in sensor capacitance resulting in an increase in the output frequency. It is observed that this decay is not very significant and it is settled within 10 min after introducing fluid.

Another set of measurements is performed to detect intermittent urination events. Two fluid pours of 100 mL each are sequentially added to the diaper on the torso, with a time gap of 10 min between them for both silver and carbon sensors. The output frequency results are tabulated in Table III. It is observed that when compared with the first pour, the second pour of fluid produced a notable change in the output frequency making it feasible to detect intermittent urination events which is a key predictor to timely diagnose of several diseases such as UTI and bladder inflammation [48]. It is observed that both silver- and carbon-printed capacitive sensors yield similar behavior in all the measurement scenarios except the level of output frequency which has been higher for the carbon sensor because of its higher sheet resistance. This leads to the development possibility of more sustainable and economical printed sensors with carbon ink when compared with silver ink.

IV. CONCLUSION

The development of smart diapers has the potential to improve healthcare services for elderly people. In this work, 65-nm bulk CMOS technology is adopted to design the power-optimized analog front-end to have battery-less operations using energy harvesting techniques. Economical and sustainable printed electronics technology is used to design the capacitive sensors on flexible substrates. The analog front-end is characterized before the integration with the printed capacitive sensors. Various in-jar and in-diaper measurement scenarios are implemented to analyze the detection and quantification of urination events in adult diapers.

The experimental results have shown that the smart diaper with printed capacitive sensor and integrated front-end is capable of detecting multiple urination events and can quantify the voided fluid volume to as low as 50 mL. An output frequency range of 5–0.7 kHz is observed with the carbon sensor over the pouring amount of 50–300-mL synthetic urine inside diaper consuming a maximum power of 3.05 μW. It is observed that the carbon sensor because of its high sheet resistance has shown higher values of output frequency for the same level of voided volume when compared with the silver sensor and exhibits similar output trends, hence enabling the development of more cost-effective sensors with carbon while promoting sustainable recycling practices. Mass production of smart diapers integrated with analog front-end and sensor using roll-to-roll printing technology is recommended for cost reduction to dispose of the system along with diapers. In future work, chemical energy harvesting from human urine [37] might be implemented to power the analog front-end for battery-less operations.

ACKNOWLEDGMENT

Technical assistance toward the printed capacitive sensors from Olli Halonen, Kim Eiroma, Mika Suhonen, Tapio Mäkelä, and Asta Pesonen is gratefully acknowledged. The authors would also like to thank Ata Golparvar and Gian Luca Barbruni, École Polytechnique Fédérale de Lausanne (EPFL), Switzerland, for their valuable review and comments.

REFERENCES

[1] *The 2021 Ageing Report: Economic and Budgetary Projections for the EU Member States (2019–2070)*, Eur. Comminssion, Brussels, Belgium, 2021, doi: 10.2765/84455.

[2] M. Goepel, R. Kirschner-Hermanns, A. Welz-Barth, K.-C. Steinwachs, and H. Rübben, "Urinary incontinence in the elderly," *Deutsches Ärzteblatt Int.*, vol. 107, pp. 531–536, Jul. 2010, doi: 10.3238/arztebl.2010.0531.

[3] G. Kellie, "Introduction to technical nonwovens," in *Advances in Technical Nonwovens*. Amsterdam, The Netherlands: Elsevier, 2016, pp. 1–17.

[4] S. Horrocks, "What prevents older people from seeking treatment for urinary incontinence? A qualitative exploration of barriers to the use of community continence services," *Family Pract.*, vol. 21, no. 6, pp. 689–696, Oct. 2004, doi: 10.1093/fampra/cmh622.

[5] K. L. Burgio, D. G. Ives, J. L. Locher, V. C. Arena, and L. H. Kuller, "Treatment seeking for urinary incontinence in older adults," *J. Amer. Geriatrics Soc.*, vol. 42, no. 2, pp. 208–212, Feb. 1994, doi: 10.1111/j.1532-5415.1994.tb04954.x.

[6] V. Lorenzo Sellarés, "Utilidad de los parámetros urinarios en la enfermedad renal crónica avanzada," *Nefrología*, vol. 39, no. 2, pp. 124–132, Mar. 2019, doi: 10.1016/j.nefro.2018.06.008.

[7] E. Bright, N. Cotterill, M. Drake, and P. Abrams, "Developing and validating the international consultation on incontinence questionnaire bladder diary," *Eur. Urology*, vol. 66, no. 2, pp. 294–300, Aug. 2014, doi: 10.1016/j.eururo.2014.02.057.

[8] M. Kohta et al., "Bacterial species distribution on the genital skin of hospitalized patients with stroke manifesting incontinence-associated dermatitis: A cross-sectional study," *Geriatrics Gerontol. Int.*, vol. 23, no. 7, pp. 537–542, Jun. 2023, doi: 10.1111/ggi.14624.

[9] S. Koudounas et al., "Bacterial invasion into the epidermis of rats with sodium lauryl sulphate-irritated skin increases damage and induces incontinence-associated dermatitis," *Int. Wound J.*, vol. 20, no. 1, pp. 191–200, Aug. 2022, doi: 10.1111/iwj.13864.

[10] Y. Mugita, S. Koudounas, G. Nakagami, C. Weller, and H. Sanada, "Assessing absorbent products' effectiveness for the prevention and management of incontinence-associated dermatitis caused by urinary, faecal or double adult incontinence: A systematic review," *J. Tissue Viability*, vol. 30, no. 4, pp. 599–607, Nov. 2021, doi: 10.1016/j.jtv.2021.07.002.

[11] J. K. Bender, J. Faergemann, and M. Sköld, "Skin health connected to the use of absorbent hygiene products: A review," *Dermatol. Therapy*, vol. 7, no. 3, pp. 319–330, Jun. 2017, doi: 10.1007/s13555-017-0189-y.

[12] T. Fujimura et al., "The influence of incontinence on the characteristic properties of the skin in bedridden elderly subjects," *Int. J. Dermatol.*, vol. 55, no. 5, pp. 234–240, Dec. 2015, doi: 10.1111/ijd.13170.

[13] M. Tanweer and K. A. I. Halonen, "Development of wearable hardware platform to measure the ECG and EMG with IMU to detect motion artifacts," in *Proc. IEEE 22nd Int. Symp. Design Diag. Electron. Circuits Syst. (DDECS)*, Apr. 2019, pp. 1–4.

[14] R. K. Albright, B. J. Goska, T. M. Hagen, M. Y. Chi, G. Cauwenberghs, and P. Y. Chiang, "OLAM: A wearable, non-contact sensor for continuous heart-rate and activity monitoring," in *Proc. Annu. Int. Conf. IEEE Eng. Med. Biol. Soc.*, Sep. 2011, pp. 5625–5628.

[15] W. Seo, W. Yu, T. Tan, B. Ziaie, and B. Jung, "Diaper-embedded urinary tract infection monitoring sensor module powered by urine-activated batteries," *IEEE Trans. Biomed. Circuits Syst.*, vol. 11, no. 3, pp. 681–691, Jun. 2017, doi: 10.1109/TBCAS.2017.2654421.

[16] Z. Ning, Z. Long, G. Yang, L. Xing, and X. Xue, "Self-powered wearable biosensor in a baby diaper for monitoring neonatal jaundice through a hydrovoltaic-biosensing coupling effect of ZnO nanoarray," *Biosensors*, vol. 12, no. 3, p. 164, Mar. 2022, doi: 10.3390/bios12030164.

[17] M. Y. E. Simik, F. Chi, R. S. I. Saleh, and A. M. S. Abdelgader, "A design of smart diaper wet detector using wireless and computer," in *Proc. World Congr. Eng. Comput. Sci.*, 2015, pp. 1–5. [Online]. Available: https://api.semanticscholar.org/CorpusID:6094738

[18] J. H. Cho et al., "A smart diaper system using Bluetooth and smartphones to automatically detect urination and volume of voiding: Prospective observational pilot study in an acute care hospital," *J. Med. Internet Res.*, vol. 23, no. 7, Jul. 2021, Art. no. e29979, doi: 10.2196/29979.

[19] I. Shitanda et al., "Self-powered diaper sensor with wireless transmitter powered by paper-based biofuel cell with urine glucose as fuel," *ACS Sensors*, vol. 6, no. 9, pp. 3409–3415, Jul. 2021, doi: 10.1021/acssensors.1c01266.

[20] J. Siden, A. Koptioug, and M. Gulliksson, "The 'smart' diaper moisture detection system," in *IEEE MTT-S Int. Microw. Symp. Dig.*, vol. 2, Jun. 2004, pp. 659–662.

[21] P. Sen, S. N. R. Kantareddy, R. Bhattacharyya, S. E. Sarma, and J. E. Siegel, "Low-cost diaper wetness detection using hydrogel-based RFID tags," *IEEE Sensors J.*, vol. 20, no. 6, pp. 3293–3302, Mar. 2020.

[22] A. Lazaro, M. Boada, R. Villarino, and D. Girbau, "Battery-less smart diaper based on NFC technology," *IEEE Sensors J.*, vol. 19, no. 22, pp. 10848–10858, Nov. 2019.

[23] M. Tekcin, E. Sayar, M. K. Yalcin, and S. K. Bahadir, "Wearable and flexible humidity sensor integrated to disposable diapers for wetness monitoring and urinary incontinence," *Electronics*, vol. 11, no. 7, p. 1025, Mar. 2022, doi: 10.3390/electronics11071025.

[24] Y. Shirahama, R. Shigeta, Y. Kawahara, T. Asami, Y. Kojima, and K. Nishioka, "Implementation of wide range soil moisture profile probe by coplanar plate capacitor on film substrate," in *Proc. IEEE SENSORS*, Oct. 2015, pp. 1–4.

[25] R. Shigeta, Y. Kawahara, G. D. Goud, and B. B. Naik, "Capacitive-touch-based soil monitoring device with exchangeable sensor probe," in *Proc. IEEE SENSORS*, Oct. 2018, pp. 1–4.

[26] R. L. D. C. Junior, E. O. Rodrigues, and R. A. R. Antayhua, "Coplanar capacitor probes design for a moisture soil sensor operating at high frequencies," in *Proc. 5th Int. Symp. Instrum. Syst., Circuits Transducers (INSCIT)*, Aug. 2021, pp. 1–6.

[27] A. Biswas, S. Yin, M. Tursunniyaz, N. KaramiMohammadi, J. Huang, and J. Andrews, "Geometrical optimization of printed interdigitated electrode sensors to improve soil moisture sensitivity," *IEEE Sensors J.*, vol. 22, no. 20, pp. 19162–19169, Oct. 2022.

[28] H. Fu, Y. Li, Z. Han, and K. Ma, "An integrated low-power and small-area time-domain dielectric chip sensor," *IEEE Sensors J.*, vol. 22, no. 11, pp. 10315–10322, Jun. 2022.

[29] J. Baek, "Smart predictive analytics care monitoring model based on multi sensor IoT system: Management of diaper and attitude for the bedridden elderly," *Sensors Int.*, vol. 4, 2023, Art. no. 100213. [Online]. Available: https://www.sciencedirect.com/science/article/pii/S2666351122000584

[30] M. Tanweer, R. Sepponen, I. O. Tanzer, and K. A. Halonen, "Development of capacitive sensors to detect and quantify fluids in the adult diaper," in *Bio-inspired Information and Communications Technologies*. Berlin, Germany: Springer, 2023, pp. 237–245, doi: 10.1007/978-3-031-43135-7_23.

[31] S. Konno, J. Kim, and K. Nakajima, "Development of capacitive sensor for diaper absorption volume," *Adv. Biomed. Eng.*, vol. 9, pp. 106–111, Jan. 2020, doi: 10.14326/abe.9.106.

[32] A. Otero, R. Fernandez, A. Apalkov, and M. Armada, "An automatic critical care urine meter," *Sensors*, vol. 12, no. 10, pp. 13109–13125, Sep. 2012, doi: 10.3390/s121013109.

[33] S. Kirchmeyer, "The OE-A roadmap for organic and printed electronics: Creating a guidepost to complex interlinked technologies, applications and markets," *Transl. Mater. Res.*, vol. 3, no. 1, Mar. 2016, Art. no. 010301, doi: 10.1088/2053-1613/3/1/010301.

[34] L. Hakola et al. (2020). *Sustainable Materials and Processes for Electronics, Photonics and Diagnostics*. [Online]. Available: https://research.lut.fi/converis/portal/detail/Publication/13340053?auxfun=&lang=en_GB

[35] Z. Tabaie and A. Omidvar, "Human body heat-driven thermoelectric generators as a sustainable power supply for wearable electronic devices: Recent advances, challenges, and future perspectives," *Heliyon*, vol. 9, no. 4, Apr. 2023, Art. no. e14707. [Online]. Available: https://www.sciencedirect.com/science/article/pii/S240584402301914X

[36] K. Liu et al., "Thermal-electric nanogenerator based on the electrokinetic effect in porous carbon film," *Adv. Energy Mater.*, vol. 8, no. 13, Jan. 2018, Art. no. 1702481, doi: 10.1002/aenm.201702481.

[37] M. Tanweer, R. Sepponen, I. Tanzer, and K. Halonen, "Sustainable printed electrodes for energy harvesting from urine to power IoT sensor nodes in smart diapers," in *Proc. 17th Int. Joint Conf. Biomed. Eng. Syst. Technol.*, 2024, pp. 65–70, doi: 10.5220/0012424100003657.

[38] M. Pulkkinen, J. Salomaa, M. M. Moayer, T. Haapala, and K. Halonen, "462-nW 2-axis gesture sensor interface based on capacitively controlled ring oscillators," in *Proc. IEEE Int. Symp. Circuits Syst. (ISCAS)*, May 2017, pp. 1–4.

[39] C. R. Paul, *Analysis of Multiconductor Transmission Lines*, 2nd ed. Hoboken, NJ, USA: Wiley, Oct. 2007.

[40] M. A. Silaghi, *Dielectric Material*. Rijeka, Croatia: InTech, Oct. 2012.

[41] *Gluespec: Industrial Adhesives and Advanced Material Data*. Accessed: Jul. 3, 2023. [Online]. Available: https://www.gluespec.com/

[42] *Dielectric Constant: Definition, Units, Formula, Plastic Values & Material List*. Accessed: Jul. 3, 2023. [Online]. Available: https://omnexus.specialchem.com/polymer-properties/properties/dielectric-constant

[43] D. C. Monga and K. Halonen, "A compact untrimmed 48ppm/°C all MOS current reference circuit," in *Proc. IEEE 65th Int. Midwest Symp. Circuits Syst. (MWSCAS)*, Aug. 2022, pp. 1–5.

[44] D. Monga, "Design of power management unit for low power socs in 65nm CMOS technology," M.S. thesis, Dept. Electron. Nanoengineering, Aalto Univ., Espoo, Finland, 2020. [Online]. Available: https://urn.fi/URN:NBN:fi:aalto-202005243275

[45] W. Jung, D. Sylvester, and D. Blaauw, "A rational-conversion-ratio switched-capacitor DC–DC converter using negative-output feedback," in *IEEE Int. Solid-State Circuits Conf. (ISSCC) Dig. Tech. Papers*, Jan. 2016, pp. 218–219.

[46] P. Favrat, P. Deval, and M. Declercq, "An improved voltage doubler in a standard CMOS technology," in *Proc. IEEE Int. Symp. Circuits Syst. (ISCAS)*, vol. 1, Mar. 1997, pp. 249–252.

[47] M. Tanweer, L. Gillan, R. Sepponen, I. O. Tanzer, and K. A. Halonen, "Evaluation of printed coplanar capacitive sensors for reliable quantification of fluids in adult diaper," in *MEDICON'23 and CMBEBIH'23*. Berlin, Germany: Springer, 2023.

[48] Y. Zhang et al., "Epidemiology of frequent/urgent urination in older adults in China: A multicenter, cross-sectional study," *Frontiers Public Health*, vol. 9, Sep. 2021, Art. no. 669070, doi: 10.3389/fpubh.2021.669070.

Muhammad Tanweer (Graduate Student Member, IEEE) received the M.Sc. degree in nano and radio sciences from Aalto University, Espoo, Finland, in 2018, where he is currently pursuing the Ph.D. degree with the Department of Electronics and Nanoengineering.

His research focuses on the design and development of IoT-based wearable biomedical sensors and systems, emphasizing sustainable, green electronics. He is dedicated to advancing the field through the integration of printed sensor interfaces, flexible ICs (FlexIC), and ultra-low-power ASIC technologies. His work aims to create self-powered, battery-less IoT sensor nodes for healthcare applications, using energy harvesting to achieve autonomous operation. This innovative approach aligns with the global shift toward sustainable technology solutions, making significant contributions to the development of green electronics and the broader IoT sensor node ecosystem.

Dipesh C. Monga (Graduate Student Member, IEEE) received the M.Sc. (cum laude) degree in micro- and nano-electronic circuit design from Aalto University, Espoo, Finland, in 2020, where he is currently pursuing the Ph.D. degree.

He was a Visiting Doctoral Researcher with the Bio/CMOS Interfaces Laboratory, École Polytechnique Fédérale de Lausanne (EPFL), Lausanne, Switzerland, for five months. His main research interests are focused on power management units and analog front-end interfaces for sensors.

Liam Gillan received the B.Sc. degree (Hons.) in pharmaceutical and chemical sciences from the University of Brighton, Brighton, U.K., in 2015, and the M.Sc. (Tech) degree in chemical, biochemical and materials engineering and the D.Sc. (Tech) in chemical engineering from Aalto University, Espoo, Finland, in 2017 and 2023, respectively.

He is a Research Scientist at VTT. During 2020, he was a Visiting Scholar in the group of Prof. Ali Javey at the University of California, Berkeley. He has authored more then ten peer reviewed journal articles and one patent application. His research interests include printed electronics and wearable devices.

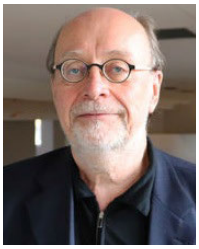

Raimo Sepponen was born on August 4, 1950. He received the D.Sc. degree in electrical engineering from Helsinki University of Technology, Espoo, Finland, in 1986.

He joined the Instrumentarium Corporation, Espoo, where he started the MRI Project. The project led to the development of an open MRI system, which is now manufactured and marketed by Philips Medical Systems. From 1992 to 1994, he was an entrepreneur who developed and manufactured medical and control systems. In 1994, he joined Helsinki University of Technology, as a Professor of Applied Electronics. The laboratory is involved in several projects related to medical electronics, including MRI, and some projects related to designing tools for electronics. He has authored more than 50 scientific papers and received patents worldwide related to more than 25 inventions.

Dr. Sepponen received the Award of Engineering from the Finnish Engineering Society in 1986, the Award of Most Significant Doctoral Thesis in Radiology from the Nordic Radiological Society, and the Award for Development of MRI from the European Society of Magnetic Resonance Imaging.

I. Oguz Tanzer (Member, IEEE) received the M.Sc. degree in electrical engineering from Middle East Technical University, Ankara, Turkey, in 1998, and the D.Sc. degree from the Helsinki University of Technology (now Aalto University), Espoo, Finland, in 2006.

From 2016, he was an Assistant Professor and the Head of the Biomedical Technology Department at the University of Health Sciences, where he established the Biomedical Technology Laboratory and lectured on medical devices and healthcare IT systems. During his industry career, he made impactful contributions at GE Healthcare, Honeywell and Ministry of Health of Turkey as a World Bank consultant. He has had an expansive career in healthcare technology, having worked in academic, engineering, and commercial roles. Recently, he has served as a fellow at Helsinki University, focusing on medical device innovation, and as the Project Director at Aalto University, leading Urisens project, Finland. Over his academic career, he has authored over 20 peer-reviewed articles in various areas of medical technology. His research at Helsinki University Hospital's Biomag Laboratory, the Laboratory of Biomedical Engineering, and the Low Temperature Laboratory at Aalto University led to the development of pioneering brain modeling tools that have significantly advanced the field.

Kari A. I. Halonen (Member, IEEE) received the M.Sc. degree in electrical engineering from Helsinki University of Technology, Espoo, Finland, in 1982, and the Ph.D. degree in electrical engineering from Katholieke Universiteit Leuven, Leuven, Belgium, in 1987.

Since 1988, he has been with the Electronic Circuit Design Laboratory, Helsinki University of Technology (since 2011, Aalto University), Espoo. Since 1993, he has also been an Associate Professor and a Full Professor with the Faculty of Electrical Engineering and Telecommunications since 1997. He became the Head of the Electronic Circuit Design Laboratory, in 1998. He was appointed as the Head of the Department of Micro- and Nanosciences, Aalto University, from 2007 to 2013. He specializes in CMOS and BiCMOS analog and RF integrated circuits, particularly for telecommunication and sensor applications. He has authored or coauthored more than 450 international and national conference and journal publications on analog and RF integrated circuits.

Dr. Halonen has served as a TPC member for ESSCIRC and ISSCC. He was a recipient of the Beatrice Winner Award in ISSCC Conference 2002. He has been an Associate Editor of IEEE JOURNAL OF SOLID-STATE CIRCUITS and IEEE TRANSACTIONS ON CIRCUITS AND SYSTEMS—I: REGULAR PAPERS, a Guest Editor of IEEE JOURNAL OF SOLID-STATE CIRCUITS, and the Technical Program Committee Chairperson of the European Solid-State Circuits Conference in 2000 and 2011.